Optics Letters

All-optical multi-channel wavelength conversion of Nyquist 16 QAM signal using a silicon waveguide

Yun Long,[1] Jun Liu,[1] Xiao Hu,[1] Andong Wang,[1] Linjie Zhou,[2] Kaiheng Zou,[3] Yixiao Zhu,[3] Fan Zhang,[3] and Jian Wang[1,*]

[1]Wuhan National Laboratory for Optoelectronics, School of Optical and Electronic Information, Huazhong University of Science and Technology, Wuhan 430074, Hubei, China
[2]State Key Laboratory of Advanced Optical Communication System and Networks, Shanghai Jiao Tong University, Shanghai 200240, China
[3]State Key Laboratory of Advanced Optical Communication Systems and Networks, Peking University, Beijing 100871, China
*Corresponding author: jwang@hust.edu.cn

Received 22 September 2015; revised 28 October 2015; accepted 28 October 2015; posted 29 October 2015 (Doc. ID 250509); published 17 November 2015

We experimentally demonstrate on-chip all-optical multi-channel wavelength conversion of Nyquist 16 ary quadrature amplitude modulation (16 QAM) signal in a silicon waveguide. The measured optical signal-to-noise ratio (OSNR) penalties of wavelength conversion are ~2 dB. The observed constellations of converted idlers indicate favorable performance of silicon-waveguide-based multi-channel wavelength conversion. We also experimentally study and compare the phase-conjugated wavelength conversion by degenerate four-wave mixing (FWM) and transparent wavelength conversion by non-degenerate FWM in the silicon waveguide.

OCIS codes: (190.4380) Nonlinear optics, four-wave mixing; (060.1660) Coherent communications.

http://dx.doi.org/10.1364/OL.40.005475

Digital signal processing (DSP) is playing an increasingly important role in coherent optical communication system for reconstructing the complex field of signal and mitigating transmission impairments [1]. It remarkably simplifies the processing of multi-level and multi-dimensional modulation format signals such as quadrature amplitude modulation (QAM). However, optical signal processing is still highly desirable for its strong abilities to overcome the electronics bottlenecks, supporting the ultrafast and transparent optical signal processing [2,3]. High-speed all-optical signal processing functions, including multiplexing, multicasting, wavelength conversion, signal regeneration, logic gate, format conversion, and tunable optical delay, would play a crucial role in achieving flexible and low-latency management of network data traffic [4]. In particular, wavelength conversion is of great importance for enhancing the reconfigurability and non-blocking capacity of future optical network, and considered to be a fundamental function facilitating advanced grooming signal processing applications [5–9].

All-optical wavelength conversions have been successfully achieved by some previous works based on optical nonlinearities in semiconductor optical amplifiers (SOAs), highly nonlinear fibers (HNLFs), and periodically poled lithium niobate (PPLN) waveguides. In [10], wavelength conversion of 16 Gbaud 16 QAM and 5 Gbaud 64 QAM was demonstrated based on four-wave mixing (FWM) in an SOA using a dual-pump configuration. Wavelength conversion of a 64 QAM signal through FWM in HNLFs was also reported in [3,11]. Moreover, using sub-band wavelength conversion, reconstruction of orthogonal frequency division multiplexing (OFDM) 8 QAM modulated super-channels was realized based on the dual pump of the orthogonal polarization scheme in HNLFs [9]. In addition, exploiting a quasi-rectangular PPLN designed by layer peeling algorithm, multi-channel wavelength conversion of QPSK with eight channels was also successfully demonstrated [12].

Silicon photonics has become one of the most promising photonic integration platforms [13]. Compared to SOAs, HNLFs, and PPLN, silicon waveguide-based wavelength converters can offer some distinct advantages: (1) in silicon waveguides, high-contrast index leads to tight light confinement, which will greatly enhance the nonlinearities; (2) silicon waveguides also feature broad bandwidth, high speed, low power consumption, and complementary metal-oxide semiconductor (CMOS) compatibility. Many previous concepts originally developed based on bulked devices could be adapted to silicon waveguides to utilize compact chip-scale applications. FWM-based wavelength conversions of 80 Gbit/s DQPSK signals [14] and 640 Gbit/s RZ-DPSK signals [15] have been demonstrated in silicon waveguides. In addition, by combining OFDM with advanced multilevel signals, on-chip all-optical wavelength conversion of multicarrier multilevel modulation signals was also demonstrated [16]. However, most of the previous works

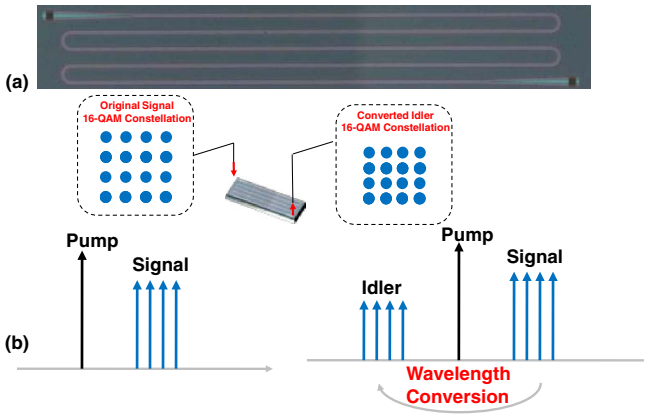

Fig. 1. (a) Photomicrograph of the silicon waveguide. (b) Schematic illustration of multi-channel all-optical Nyquist 16 QAM signal wavelength conversion in a silicon waveguide.

focus on single-channel operation. Beyond single-channel operation, multi-channel wavelength conversion operation is also highly desired. In addition, Nyquist pulse shaping signal has recently attracted increasing interest for efficient spectral usage [17]. In this scenario, silicon waveguide-based multi-channel wavelength conversion of Nyquist pulse shaping signals is highly desirable.

In this Letter, we fully explore multi-channel all-optical wavelength conversion using Nyquist 16 QAM signal based on a silicon waveguide. Low-penalty wavelength conversion of a 5 Gbaud multi-channel Nyquist 16 QAM signal is demonstrated in the experiment. Moreover, degenerate four-wave mixing (DFWM) for phase-conjugated wavelength conversion and non-degenerate four-wave mixing (NFWM) for transparent wavelength conversion are experimentally studied.

The silicon waveguide employed in the experiment is a 6 mm long silicon-on-insulator (SOI) waveguide with dimensions of 500 nm width and 220 nm thickness. Vertical grating couplers are used to couple light in/out of the silicon waveguide and ensure operation with TE-polarized light. The grating coupling loss is about 7 dB per facet. The photomicrograph of the silicon waveguide is shown in Fig. 1(a). Figure 1(b) depicts the wavelength conversion process based on DFWM in a silicon waveguide. One continuous-wave (CW) pump and four-channel Nyquist 16 QAM data carrying signal are fed into the silicon waveguide. When propagating along the silicon waveguide, pump photons are annihilated to create signal photons and newly converted idler photons by the FWM process. At the output of the silicon waveguide, data information carried by the input signal is converted to the idler.

Figure 2 shows the experimental setup. At the transmitter, the CW outputs from four external cavity laser (ECL1-4) serve as the multi-channel signal light for the FWM. The signal light is then modulated with Nyquist 16 QAM at 5 Gbaud by an optical I/Q modulator. The modulated 5 Gbaud multi-channel Nyquist 16 QAM signal is then amplified by an erbium-doped optical fiber amplifier (EDFA1) followed by a tunable filter (TF1) to suppress the amplified spontaneous emission (ASE) noise. Afterward, the four-channel Nyquist 16 QAM signal is combined with another CW light from ECL5 serving as the pump light through a coupler. For NFWM, an additional pump light ECL6 is also coupled together with the signal. The combined signal and pump are then amplified using anther EDFA (EDFA2) before being launched into the silicon chip. Polarization controllers (PC5, PC6, and PC7) in Fig. 2 are used to adjust the polarization states of the four-channel Nyquist 16 QAM signal and pump to achieve optimized conversion efficiency. After the wavelength conversion, the desired idler is selected using two-stage optical filtering (TF2, TF3). First, the desired idler is selected using TF2. Since the power level of the idler is relatively low, the selected idler is amplified by EDFA3. Second, to suppress the ASE noise originated from the EDFA3, another TF3 is employed. The CW output from ECL7 serves as a reference light for coherent detection. The receiver is based on a coherent mixer and a high-speed real-time oscilloscope to capture the signals. The offline postprocessing can be briefly summarized as follows [18]. The carrier frequency recovery is conducted by a phase increment estimation algorithm. After the carrier frequency recovery, a matched receiving root-raised-cosine (RRC) filter is adopted to satisfy the first Nyquist criterion. The signals are then resampled to two samples per symbol, and the training sequences are picked up for linear channel estimation and equalization. With linear channel estimation and equalization, time domain finite impulse response (FIR) filtering is extracted from training

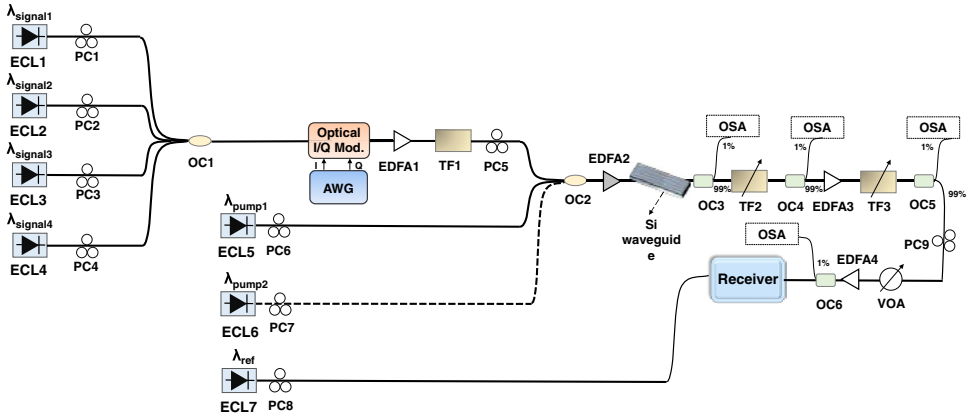

Fig. 2. Experimental setup for all-optical multi-channel wavelength conversion of Nyquist 16 QAM signals in a silicon waveguide. ECL, external cavity laser; AWG, arbitrary waveform generator; PC, polarization controller; TF, tunable filter; EDFA, erbium-doped fiber amplifier; OC, optical coupler; VOA, variable optical attenuator; OSA, optical spectrum analyzer.

sequences and convoluted with the data. The phase is corrected with pilots, and then estimated with the blind phase search (BPS) algorithm.

In the experiment, the wavelengths of the four-channel signal are 1552.5, 1552.1, 1551.7, and 1551.3 nm, respectively. The pump light is 1549.3 nm. The measured DFWM-based multi-channel wavelength conversion spectrum after the silicon waveguide is shown in Fig. 3. For a DFWM process, the angular frequency of the generated idler light can be written as $\omega_{idler} = 2\omega_{pump} - \omega_{signal}$; thus, the wavelengths of the converted idlers are 1547.3, 1546.9, 1546.5, and 1546.1 nm, respectively, which can be clearly seen in Fig. 3.

We define the conversion efficiency as the power ratio of converted idler to signal. Figure 4(a) shows the measured conversion efficiency as a function of the pump power at $\lambda_{pump} = 1549.3$ nm. The pump light power here is the collected power in the silicon waveguide taking into account the coupling loss of the grating coupler. It can be seen that the conversion efficiency increases with the pump power. ~ – 24.5 dB conversion efficiency is observed when the pump light power is 17.7 dBm, and the signal wavelength is 1551.3 and 1551.7 nm. The converted idler wavelength also can be tuned simply by changing the pump wavelength. The measured conversion efficiency as a function of pump light wavelength is shown in Fig. 4(b). The pump light power is fixed at 16.7 dBm.

The measured bit-error rate (BER) curves as a function of optical signal-to-noise ratio (OSNR) are shown in Fig. 5. The observed OSNR penalty is around 1.8 dB at a BER of 2×10^{-3} (enhanced forward error correction (FEC) threshold) for Nyquist 16 QAM wavelength conversion with the converted idler at 1546.1 and 1546.5 nm. The received OSNR penalties are about 2.7 dB for converted idlers at 1546.9 and 1547.3 nm. The increased OSNR penalty is mainly due to the reduced conversion efficiency for converted idlers at 1546.9 and 1547.3 nm.

We further compare the wavelength conversions of Nyquist 16 QAM signal based on NFWM and DFWM processes. Single channel operation is examined in the experiment. For NFWM, the two pump wavelengths are selected to be 1549.3 and 1552.5 nm. The signal wavelength is 1551.5 nm. The measured NFWM spectrum after the silicon waveguide is shown in Fig. 6. For DFWM, the pump wavelength is 1549.3 nm and the signal wavelength is 1552.5 nm. The measured DFWM spectrum after the silicon waveguide is shown in Fig. 7.

For DFWM, the complex field of idler is $A_{idler} = A_{pump}^2 A_{signal}^*$, where A_{pump} and A_{signal} are the complex fields

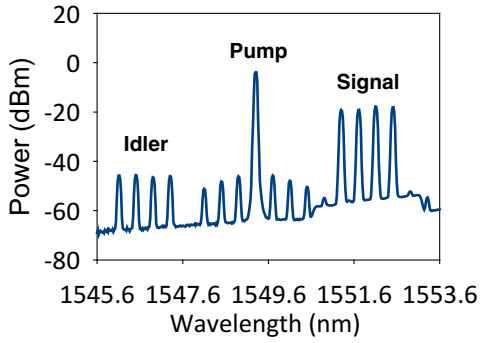

Fig. 3. Measured DFWM-based multi-channel wavelength conversion spectrum after the silicon waveguide.

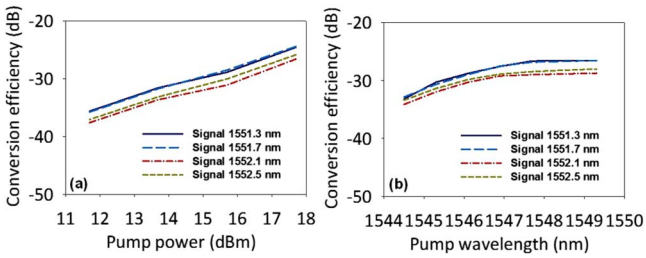

Fig. 4. (a) Conversion efficiency versus pump power when the pump wavelength is 1549.3 nm. (b) Conversion efficiency vs pump wavelength.

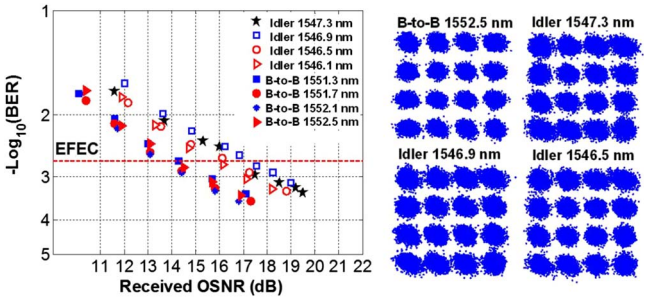

Fig. 5. Measured BER curves and constellations for all-optical multi-channel wavelength conversion of Nyquist 16 QAM signal.

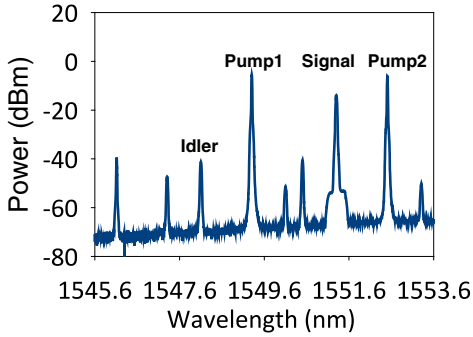

Fig. 6. Measured NFWM spectrum after the silicon waveguide.

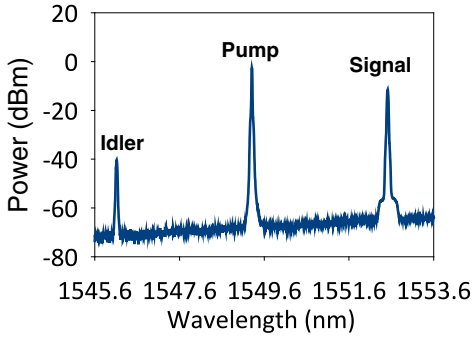

Fig. 7. Measured DFWM spectrum after the silicon waveguide.

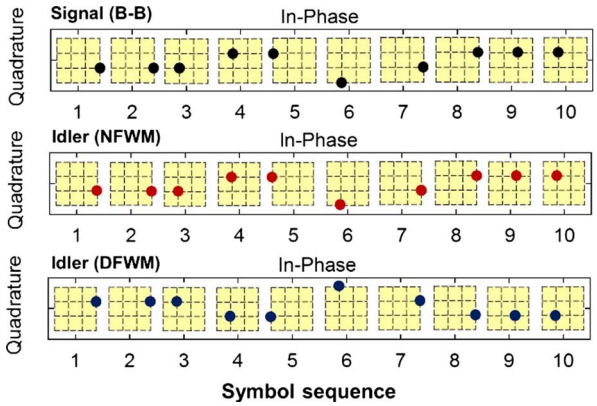

Fig. 8. Measured symbol sequence of converted idlers by NFWM and DFWM, and the original signal.

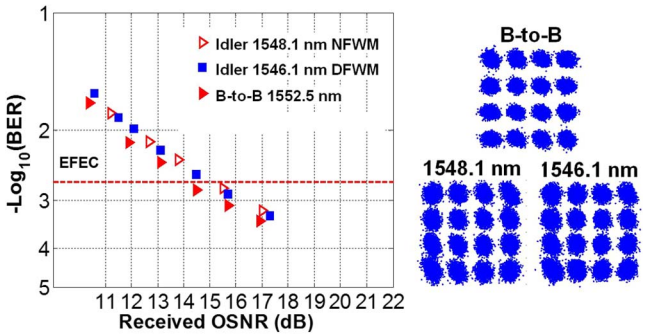

Fig. 9. Measured BER curves and constellations for single-channel DFWM-based phase-conjugated wavelength conversion and NFWM-based transparent wavelength conversion of Nyquist 16 QAM signals.

of pump and input signal, respectively [19,20]. The idler is proportional to the conjugation of the input signal while, for NFWM, the complex field of idler can be written as $A_{\text{idler}} = A_{\text{pump1}} A^{*}_{\text{pump2}} A_{\text{signal}}$. The idler is proportional to the input signal. To verify the phase conjugated wavelength conversion by DFWM and transparent wavelength conversion by NFWM, we measure the symbol sequence of converted idlers by DFWM and NFWM and original signal (B-B), as shown in Fig. 8. One can clearly see from Fig. 8 that the converted idler by DFWM flips constellation points in the complex I/Q plane with respect to the I-axis, corresponding to the phase conjugation of the original Nyquist 16 QAM signal. In contrast, the converted idler by NFWM recovers the constellation of the original signal, corresponding to the transparent wavelength conversion of the original Nyquist 16 QAM signal.

The measured BERs as a function of OSNR for single-channel wavelength conversion based on NFWM/DFWM are shown in Fig. 9. The observed OSNR penalty is around 1 dB at a BER of 2×10^{-3} (EFEC threshold) for both NFWM and DFWM wavelength conversions.

In summary, we demonstrated DFWM-based multi-channel all-optical wavelength conversion of Nyquist 16 QAM signal using a silicon waveguide. We also studied and compared the DFWM-based phase-conjugated wavelength conversion and NFWM-based transparent wavelength conversion in the experiment. The received OSNR penalties are measured to be ~2 dB for DFWM-based multi-channel wavelength conversion and ~1 dB for both single-channel DFWM-based phase-conjugated wavelength conversion and single-channel NFWM-based transparent wavelength conversion. To further improve the conversion efficiency, several possible ways might be considered as follows: (1) optimize the dispersion of the waveguide to better satisfy the phase matching condition of FWM process, (2) optimize the coupling efficiency of the grating coupler to ensure more light coupled into the waveguide, and (3) employ the reverse-biased p-i-n diode structures across the waveguide to suppress the nonlinear absorption in the waveguide.

Funding. National Natural Science Foundation of China (NSFC) (11274131, 11574001, 61077051, 61222502); Program for New Century Excellent Talents in University (NCET) (NCET-11-0182); Wuhan National Laboratory for Optoelectronics (WNLO); Wuhan Science and Technology Plan Project (2014070404010201).

REFERENCES

1. C. Laperle and M. O'sullivan, J. Lightwave Technol. **32**, 629 (2014).
2. A. E. Willner, S. Khaleghi, M. R. Chitgarha, and O. F. Yilmaz, J. Lightwave Technol. **32**, 660 (2014).
3. G.-W. Lu, T. Sakamoto, and T. Kawanishi, Opt. Express **22**, 15 (2014).
4. X. Wu, *Asia Communications and Photonics Conference* (Optical Society of America, 2012), paper AS2G. 4.
5. S. J. B. Yoo, J. Lightwave Technol. **14**, 955 (1996).
6. J. M. H. Elmirghani and H. T. Mouftah, IEEE Commun. Mag. **38**(3), 86 (2000).
7. T. Durhuus, B. Mikkelsen, C. Joergensen, S. L. Danielsen, and K. E. Stubkjaer, J. Lightwave Technol. **14**, 942 (1996).
8. S. Subramaniam, M. Azizoglu, and A. K. Soman, IEEE/ACM Trans. Netw. **4**, 544 (1996).
9. S. You, C. Li, Q. Yang, M. Luo, Y. Qiu, X. Xiao, and S. Yu, IEEE Photon. Technol. Lett. **26**, 801 (2014).
10. B. Filion, W. Ng, A. T. Nguyen, L. A. Rusch, and S. LaRochelle, Opt. Express **21**, 19825 (2013).
11. A. H. Gnauck, E. Myslivets, M. Dinu, B. P. P. Kuo, P. Winzer, R. Jopson, N. Alic, A. Konczykowska, F. Jorge, and J.-Y. Dupuy, *European Conference and Exhibition on Optical Communication* (Optical Society of America, 2012), paper Th.2.F.2.
12. A. Albuquerque, B. J. Puttnam, M. Drummond, S. Shinada, R. Nogueira, and N. Wada, *Optical Communication (ECOC 2013), 39th European Conference and Exhibition on* (IET, 2013), paper P.2.10.
13. W. Bogaerts, R. Baets, P. Dumon, V. Wiaux, S. Beckx, D. Taillaert, B. Luyssaert, J. Van Campenhout, P. Bienstman, and D. Van Thourhout, J. Lightwave Technol. **23**, 401 (2005).
14. M. A. Ettabib, K. Hammani, F. Parmigiani, L. Jones, A. Kapsalis, A. Bogris, D. Syvridis, M. Brun, P. Labeye, and S. Nicoletti, Opt. Express **21**, 16683 (2013).
15. H. Hu, H. Ji, M. Galili, M. Pu, C. Peucheret, H. Christian, H. Mulvad, K. Yvind, J. M. Hvam, P. Jeppesen, and L. K. Oxenløwe, Opt. Express **19**, 19886 (2011).
16. C. Li, C. Gui, X. Xiao, Q. Yang, S. Yu, and J. Wang, Opt. Lett. **39**, 4583 (2014).
17. Z. Zheng, R. Ding, F. Zhang, and Z. Chen, Opt. Express **21**, 17505 (2013).
18. F. Zhang, D. Wang, R. Ding, and Z. Chen, Opt. Express **22**, 23415 (2014).
19. J. Wang, S. R. Nuccio, J.-Y. Yang, X. Wu, A. Bogoni, and A. E. Willner, Opt. Lett. **37**, 1139 (2012).
20. J. Wang, J.-Y. Yang, H. Huang, and A. E. Willner, Opt. Express **21**, 488 (2013).